Journal of Signal Processing, Vol. 13, No. 2, pp. 133-144, March 2009

PAPER

# A Bio-Inspired Image Processor for Edge Detection with Single-Electron Circuits

Andrew Kilinga Kikombo[1], Alexandre Schmid[2], Tetsuya Asai[1], Yusuf Leblebici[2] and Yoshihito Amemiya[1]

[1]Department of Electrical Engineering, Hokkaido University
Kita 13, Nishi 9, Kita-ku, Sapporo, 060-0814, Japan
[2]Microelectronic Systems Laboratory, Swiss Federal Institute of Technology (EPFL)
Lausanne, CH-1015, Switzerland
E-mail address: kikombo@sapiens-ei.eng.hokudai.ac.jp

**Abstract** **We propose a neuromorphic single-electron structure that performs edge detection in incident images. Edge detection is a primary function carried out in the vertebrate retina. Several edge-detecting circuits based on a well studied model of edge detection in the vertebrate retina have been proposed and implemented with CMOS LSIs [1] - [3]. In this paper, based on the same model, we propose a possible single-electron architecture and show that it can detect or enhance edges in incident images. We constructed one- and two-dimensional artificial retinas with the proposed subcircuits and confirmed their basic operation through Monte-Carlo based computer simulations.**

**Keywords:** single-electron, artificial retina, edge detection, neuromorphic LSIs

## 1. Introduction

Over the past three decades, achieving faster and more efficient electronic systems has been realized though miniaturization of the transistor. With the present device processing technologies, the transistor sizes have shrunk to the two-digit nano meter scale making transistors vulnerable to "nano-scale" physical characteristics. At the same time, improvements in device fabrication technologies have made it possible to fabricate quantum devices, such as single-electron devices.

Single-electron circuits can be considered as highly functional units both in digital and analog computational systems [4] because they inherently operate with extreme low power dissipation, and provide a high integration density per unit area. Thus far, a number of single-electron circuits , based on conventional Boolean circuit architectures have been proposed [5]. However, the reliability of Boolean-based architecture schemes remains questionable due to the non-uniformity of single units, the low number of electrons representing unit logic bits, and low tolerance against environmental noises. A possible method toward solving these drawbacks could be attained by employing neuromorphic-based circuit architectures in creating single-electron circuits. Despite that, individual biological neurons are sensitive to noises (low defect tolerance), operate asynchronously due to structural differences, and have enormous time jitters in signal transmission [8] - [7], their networks are robust to external interference, and successfully process information (see [13] - [15] and references therein). Therefore, with hints from neuronal information processes, we could find a breakthrough to the shortcomings facing electronic circuits consisting of single-electron devices.

Electrical circuits that are designed by mimicking computational structures in living organisms–*neuromorphic circuits*, would provide insights into developing even more efficient processors for parallel information processing applications [16]. As an example of neuromorphic systems, edge detecting LSIs have been extensively studied [1]. Edge detection is a primary function in the early stages of visual processing carried out in the vertebrate retina. Thus far, only neuromorphic circuits achieved with silicon have been designed and fabricated [1] - [3]. In this work, we propose a possible image-processing structure for single-electron circuits as an example toward linking *nano-electronic devices* with *neuromorphic architectures*. Based on a well studied model of the vertebrate inner retina, this paper proposes a single-electron circuit that detects edges, and investigates its basic operations.

In the sections that follow, we will start by explaining the model, then give details on how to implement it with single-electron devices. Finally, we give details on the operation of our circuit with one- and two-dimensional circuit constructions.

## 2. The model

The vertebrate retina consists of massively interconnected neural cells in a hierarchical structure, where edge detection

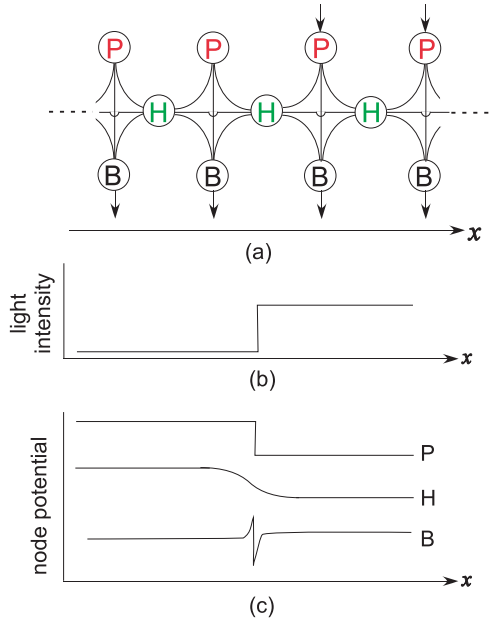


Fig. 1 Cross section of the vertebrate retina, showing neurons involved in edge detection: (a) Model: P—Photoreceptors, H—Horizontal cells, and B—Bipolar cells. (b) Intensity profile of incident light and (c) Potentials of P, H, and B cells, showing response to the incident light (input)

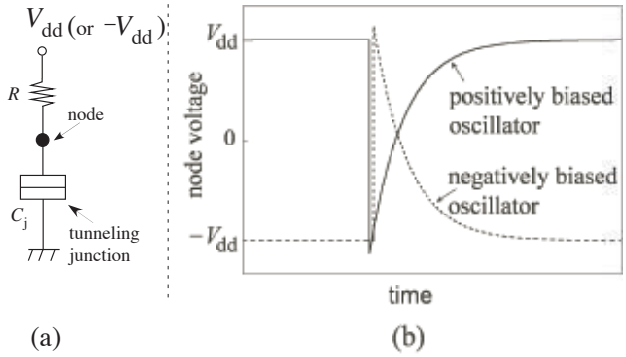


Fig. 2 Single electron oscillator: (a) Circuit configuration (b) Monostable, or one-shot, operation of positively biased (solid curve) and negatively biased (dashed curve) oscillators

is carried out mainly through three types of cells: (i) photoreceptors that transduce light inputs into electrical signals, (ii) horizontal cells that receive inputs from the superjacent layer of photoreceptors and produce spatially averaged outputs in relation to the inputs, and (iii) bipolar cells that produce the difference in amplitudes between the outputs of photoreceptors and horizontal cells. The schematic model is shown in Fig. 1(a) . In this model, we assume that illuminated (or non-illuminated) photoreceptors produce low (or high) potentials (Figs. 1(b) and (c)-P). The outputs are spatially averaged by horizontal cells (Fig. 1(c)-H). The bipolar cells detect the position of edges in the incident images by producing the difference in amplitudes between photoreceptors and horizontal cells. This is obtained by subtracting "H"- from their corresponding "P"-values in bipolar cells. Therefore, the non-zero outputs of bipolar cells represent the positions of edges in the input image (Fig. 1(c)-B).

## 3. Implementation with Single-Electron Devices

In this section we propose a neuromorphic architecture, based on the retinal model above, with single-electron oscillators. We start by giving details on how to realize the constitutive elements, i.e., photoreceptors, horizontal and bipolar cells with single electron devices, and then explain the configuration of a unit pixel circuit.

### 3.1 Single-electron oscillator

The proposed circuit is implemented with single-electron oscillators. A single-electron oscillator, shown in Fig. 2(a), is a simple circuit consisting of a tunneling junction $C_j$ and high resistance $R$ connected in series at the node (•) and biased with a positive voltage $V_{dd}$ (Fig. 2(a)) or a negative voltage $-V_{dd}$ . It operates as a relaxation oscillator at low temperatures at which the Coulomb-blockade effect takes place. The oscillator is astable if the bias voltage $V_{dd} > e/(2C_j)$ (e is the elementary charge) and monostable if $V_{dd} < e/(2C_j)$ (see [19] - [18] for a detailed explanation). The node voltage of the monostable oscillator is equal to the bias voltage in an equilibrium state, and no change occurs under that condition. Upon application of an external trigger signal, such as incidence of photons, the Coulomb blockade is broken off, and electron tunneling occurs through the tunneling junction. The node voltage of a positively biased oscillator drops by $e/C_j$, because of tunneling from the ground to the node, then gradually increases to return to $V_{dd}$ as junction capacitance $C_j$ is charged through resistance $R$ (Fig. 2(b)-solid curve). In a negatively biased oscillator, the node voltage jumps by $e/C_j$ because of tunneling from the node to the ground, and then gradually decreases to return to $-V_{dd}$ (Fig. 2(b)-dashed curve).

### 3.2 Photoreceptor circuit

Photoreceptors convert incident light inputs into electrical signals. We implement a retinal photoreceptor with a positively biased monostable oscillator that is triggered by external light inputs. In the absence of external inteference (thermal or incoming photons) the node voltage of the oscillator is stable (and equivalent to the bias voltage). If a photon (light) is illuminated on the nano-dot, *photo-induced charging effect* ([20],[21]) occurs and an electron tunneling is induced from the ground to the nano-dot across the tunneling junction. Therefore the oscillator changes its node voltage from positive to negative. Since the intensity of input light is proportional to the number of incident photons, the number of tunneling and recharging events also increase. Therefore the intensity of incoming light would correspond to the average tunneling rate in the photoreceptors. To realize the photoreceptor layer, we use a single oscillator for a single photoreceptor cell.

### 3.3 Horizontal cell circuit

The horizontal cell layer receives inputs from the superjacent layer of photoreceptors to produce a spatially averaged output. The horizontal cells are implemented with negatively biased single-electron oscillators. Fig. 3 shows the configuration of the horizontal cell layer. The extensive gap junctions in the retinal cells are emulated by a resistive-coupling, realized through resistor $R_h$, between neighboring horizontal oscillators. If tunneling takes place in one of the horizontal cell circuits, from the node to the ground, the node voltage of the corresponding oscillator changes from a low to a high value. Through this resistive coupling, the excess negative charge is redistributed to neigboring horizontal cells, reducing their node voltages. The change in the node voltage is inversely proportional to the spatial distance from the tunneling cell: oscillators nearest to the tunneling cell experience a higher drop in their node voltages, and therefore have a higher probability of tunneling than those positioned further. Thus, the average tunneling rate decreases with the spatial distance from the tunneling cell. Therefore, negatively biased oscillators coupled through resistances would produce a spatially weighted output in relation to the input from superjacent photoreceptor cells.

### 3.4 Bipolar cell circuit

Bipolar cells detect the position of edges by producing the difference in the amplitude of corresponding photoreceptors and horizontal cells. In conventional silicon retinas, this could be realized with an operational amplifier or current subtraction method. To implement a similar architecture with single-electron devices, we would require a complicated circuit. We therefore, qualitatively imitated the subtractive functions of the bipolar cells through neural shunting inhibition mechanism.

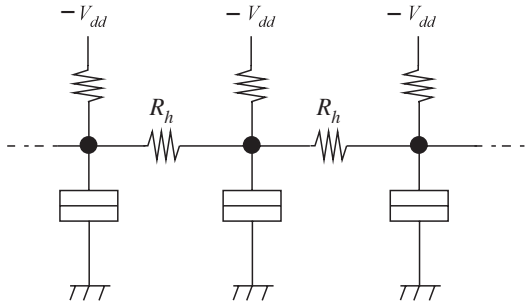


Fig. 3 Configuration of the horizontal cell layer: A single horizontal cell is implemented with a negatively biased oscillator, while the junction gaps are emulated through resistive coupling realized with resistor $R_h$

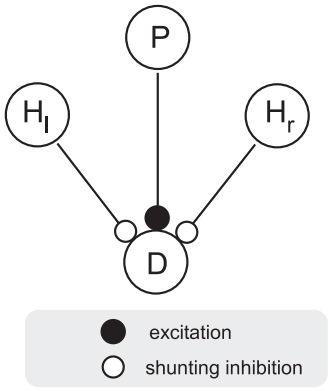


Fig. 4 Conceptual configuration of bipolar cells: Neural excitation and inhibition

This mechanism is illustrated in Fig. 4. We consider a configuration in which the photoreceptors (P) produce an excitatory signal, while the horizontal cells ($H_l$ and $H_r$) produce an inhibitory signal toward "D" cells. If the excitatory signal surpasses the inhibitory signal in amplitude, it triggers cell "D" to tunnel (excitation). Otherwise, cell "D" would be restrained from tunneling (shunting inhibition).

These two mechanisms can be achieved with single-electron devices through capacitive couplings [22]-[24]. An excitatory coupling is achieved by connecting a positively (+) biased oscillator to one that is negatively (-) biased. In the absence of an external input, the oscillator node takes a voltage value equivalent to the bias voltage. If tunneling occurs

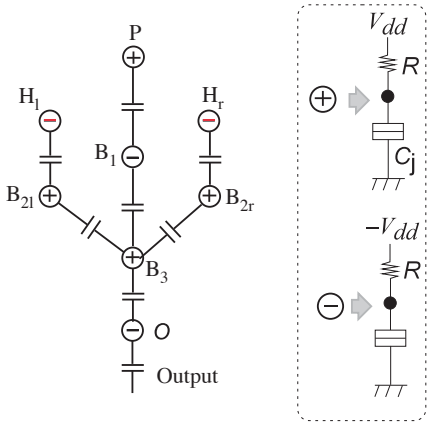


Fig. 5 Realizing the bipolar circuit: Neural excitation and inhibition with single-electron circuits

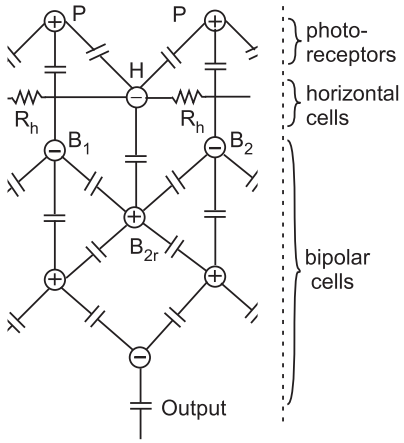


Fig. 6 Configuration of a unit pixel of the edge detecting circuit consisting of "P", "H", and "B" circuit blocks

in the positive oscillator, through the capacitive coupling, the negative charge leads to a drop in the node potential of the coupled negative oscillator below its threshold, thus inducing it to tunnel. Shunting inhibition is realized by applying the same bias voltage to two coupled oscillators. For example, if the two are positively biased, tunneling in either of them leads to a drop in the node voltage of the other far below the threshold, thus restraining it from tunneling (inhibition) even in the presence of an external trigger input.

Fig. 5 shows fundamental circuits for neural excitation and inhibition with single-electron oscillators. Let us assume that electron tunneling occurred in "P". This triggers a signal flow along the middle branch: electron tunneling in "P" leads to a drop in the node voltage of $B_1$ below its threshold (thus inducing it to tunnel). $B_1$ in turn induces tunneling in $B_3$, and tunneling in "*O*" is consequently induced (excitation). On the other hand if tunneling takes place in cells $H_l$ and $H_r$, this triggers subsequent tunneling in the left and right branches. Tunneling in $B_{2l}$ and $B_{2r}$ decreases the node voltage of $B_3$ restraining it from tunneling (shunting inhibition)–in other words, tunneling in "H" cells blocks excitatory signals initiating from "P" in the middle branch. If tunneling occurs in either of the "H" cells, this would not have a sufficiently large inhibitory effect on $B_3$, and the probability of electron tunneling taking place (tunneling rate) would be higher than that in the previous case. With these excitatory and inhibitory configurations, we partly imitate the subtractive functions of bipolar cells.

### 3.5 Configuration of a unit pixel

The edge detecting circuit is constructed with "P", "H", and "B" blocks, proposed in the preceding section. The configuration of a unit pixel is shown in Fig. 6. To increase the inhibitory effect of the horizontal cell layer, additional excitatory coupling was introduced between $B_{1,2}$ and $B_{2r}$.

## 4. Simulation Results

To confirm the basic operation, we constructed (i) a one-dimensional array retinal-circuit consisting of 100 pixel circuits, and (ii) a two-dimensional retinal-circuit consisting of $100 \times 100$ pixel circuits. We carried out Monte-Carlo based simulations: transient responses of the "P", "H", and "B" cell circuits, edge responses, sensitivity to light intensity, Mach bands and evaluated signal to noise ratio (SNR) with temperature, to confirm their basic operations. In the simulations, the horizontal layer gap junction was simulated with a resistance $R_h = 400$ MΩ, excitatory and inhibitory capacitive coupling with a capacitance of 2 aF, tunneling junction capacitance $C_j$, series resistance $R$, and tunneling junction conductance were set to 10 aF, 100 MΩ, and 1 μS respectively. The simulation time was 700 ns.

### 4.1 One-dimensional array circuit

The projected image is shown in Fig. 7. The dark region shows non-illuminated regions of the array, while the unshaded region (pixels 33-67) represents uniformly illuminated photoreceptors.

Light input was simulated by applying an external trigger input (whose frequency is equivalent to the intensity of the input light) to corresponding photoreceptors. In this simulation, the applied trigger frequency and amplitude were set to 110 MHz, and 2.5 mV respectively.

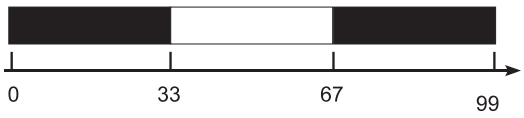


Fig. 7 Binary image projected onto the one-dimensional retinal circuit

#### 4.1.1 Transient responses

Fig. 8 shows the time-course responses of photoreceptors, horizontal and bipolar cell circuits. Fig. 8(a) shows the response of the 50*th* photoreceptor circuit. The photoreceptor receives a series of trigger signals, which induce it to tunnel from a high to a low voltage, followed by recharging to repeat the same cycle. We refer to each of these cycles as a firing event. The light intensity is computed by calculating the average firing rate of each photoreceptor circuit. Fig. 8(b) shows the response of the 50*th* cell of the subjacent horizontal cell layer. As mentioned in the previous section, due to the averaging effect of gap junctions, the firing rate of horizontal cell circuits is somewhat lower than that of corresponding photoreceptor circuits. Figs. 8(c) and (d) show the responses of the 50*th* (middle of the illuminated region) and 33*rd* (left edge) bipolar cell circuits respectively. Note that the firing rate of circuits within the illuminated region (Fig. 8:(c)) is not zero, however, it is extremely low compared to the edge cells. The simulations were carried out at T = 0 K.

#### 4.1.2 Edge response

Figs. 9(a), (b) and (c) correspond to the average tunneling rates for photoreceptors, horizontal and bipolar cell layers. The vertical axes are normalized by the maximum average firing rate in the photoreceptor layer. As mentioned in the preceding section, the average firing rate of the horizontal cells is somewhat lower than that of the photoreceptors. The image edges correspond to the high firing positions of the bipolar cell circuit. However, the firing rates of bipolar cells within the illuminated region have a comparatively low non-zero output.

#### 4.1.3 Sensitivity to light intensity

The firing rate of photoreceptors would be proportional to the intensity of input light (section 3.2). To simulate the response of our circuit to various light intensities, we altered the frequency of the applied input pulse trigger, and computed the average tunneling rates of bipolar cells. The results are shown in Fig. 10. The maximum response frequency was 110 MHz, determined by the minimum charging period within ”P”, ”H”, and ”B” cell layer oscillators.

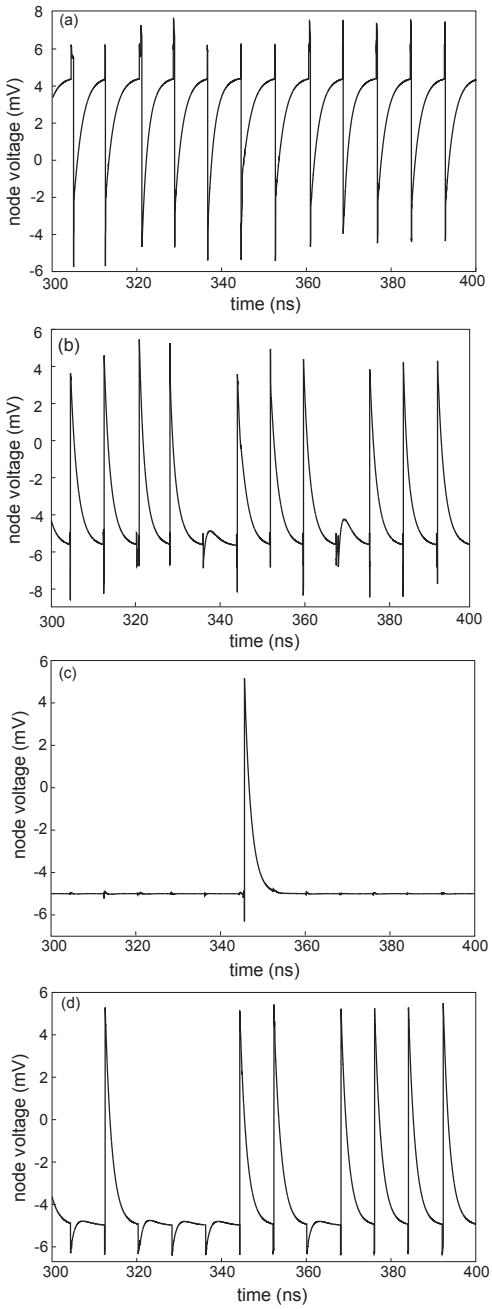


Fig. 8 Transient responses of constitutive circuit cells: (a) Photoreceptors, (b) Horizontal cells, (c), and (d) Bipolar cell circuits. (c) shows the response of bipolar cells in the middle of illuminated region, while (d) shows response of those in the edges of the illuminated region. The simulation temperature T = 0 K

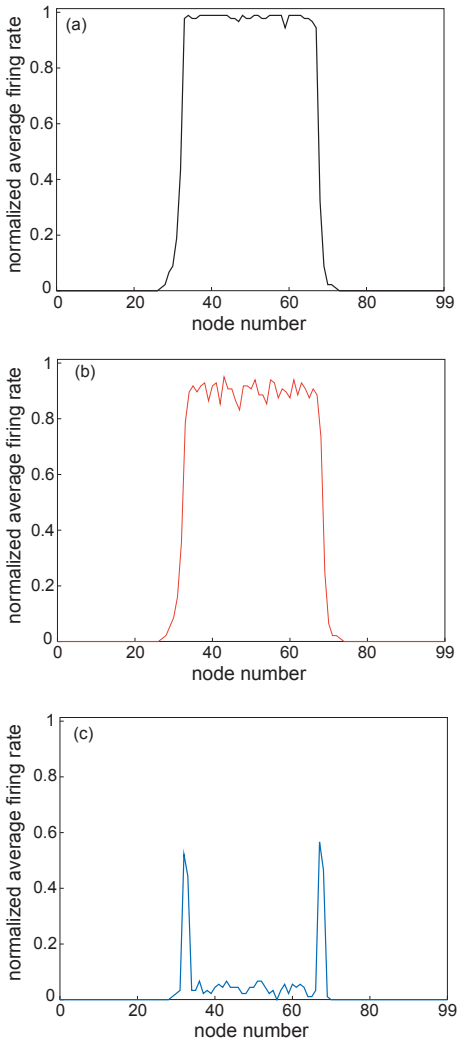


Fig. 9 Response to input images: (a) Average firing rate for photoreceptors—input, (b) Average firing rate for horizontal cells, and (c) Average firing rate of bipolar cells—output (T = 0 K)

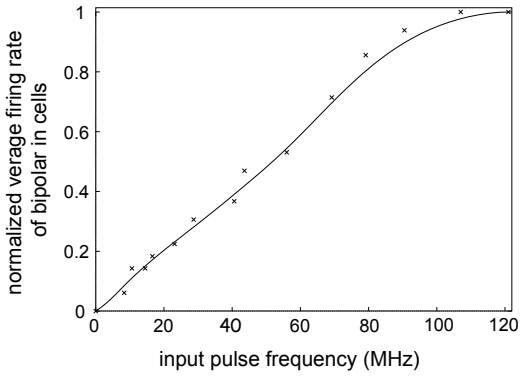


Fig. 10 Response to light intensity, simulated by varying frequency of input trigger signal—horizontal axis: The vertical axis represents the maximum firing rate of edge cell circuits, normalized by the firing rate for maximum light intensity (frequency = 110MHz). Simulated at T = 0 K

#### 4.1.4 Mach bands

Mach bands are defined as illusory light or dark bands that appear when a spatial ramp in light intensity (in projected images) abruptly changes slope [1],[25] . To confirm the Mach-band response of our circuit, the ramp input shown in Fig. 11(a) was fed to the photoreceptor layer. The input was simulated by setting the frequency of the input trigger signal at 10MHz for photoreceptors between nodes 0 and 33, ramp increment between nodes 33 and 67 from 10 MHz to 110 MHz and a constant frequency of 110 MHz for nodes 68-99. The response of the bipolar cell circuit layer (output) is shown in Fig. 11(b). The vertical axis is normalized by the firing rate for maximum light intensity (frequency = 110MHz). The circuit could detect the abrupt change in slope of input light intensity. This is shown in Fig. 11(b)-"peak", at node positions "33" and "67".

#### 4.1.5 Temperature characteristics

The temperature characteristics were evaluated by computing the circuit's ability to detect edges with increasing temperatures. Figs. 12 (a)-(c) show edge responses at T = 0 K, T = 10 K, and T= 20 K respectively. The vertical axes are normalized by the maximum firing rate in the bipolar cell layer at T = 0 K. As the temperature increases, the overall tunneling rates within the circuit increase, leading to a decrement in its ability to detect edges. The ability to detect edges was evaluated as the peak signal to noise ratio (PSNR). To evaluate the overall performance against temperature, the PSNR is defined as:

$$\mathrm{PSNR} = 20\log_{10}\left(\frac{f_{\max}}{\sqrt{\mathrm{MSE}}}\right) \quad (1)$$

$$\mathrm{MSE} = \frac{1}{N}\sum_{i=0}^{N-1}(f_0(i) - f_T(i))^2$$

where, $f_{\max}$ is the average firing rate for the entire bipolar circuit at room temperature, MSE is the mean square error, $f_0(i)$ is the firing rate of the ith node of the bipolar circuit at zero temperature (i.e., the ideal output), and $f_T(i)$ is the firing rate for the ith node of the bipolar circuit at temperature

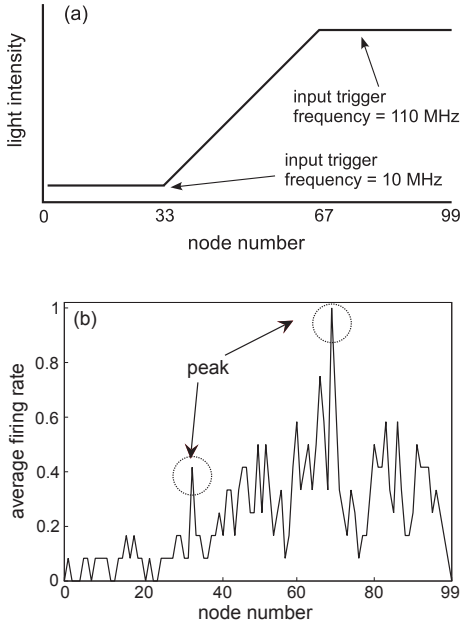


Fig. 11 Mach band: (a) Light intensity profile of input image, and (b) Response—average firing rate for bipolar cells (T = 0 K)

T K, and $N = 100$. The MSE at each temperature was calculated by averaging five runs. The firing rate $f_{\max}$ was 8.33, normalized by the maximum firing rate at 0 K.

Fig. 13 shows the PSNR over a temperature range between 0 and 50 K. The circuit could detect edges with a contrast ratio of 23 dB at T = 5 K. This is presumed to be low in comparison to the capacity of the vertebrate retina, (and other electronic systems) in the range of 20 - 40 dB at higher temperatures. This could be attributed to the fact that besides inhibitory mechanisms, there could be other mechanisms involved in edge detection in actual retinas, as compared to our circuit that only modeled inhibition mechanisms [27]-[26]. These could also include stochastic resonance [29], [30], aggregating and thresholding mechanisms together with higher-level visual information processes found in biological systems. Therefore, we think that the PSNR of our circuit could be improved if we were able to incorporate all these mechanisms. A possible architectural approach that could be used to improve performance against temperature, hence PSNR in the proposed circuit, is discussed in section 5.2.

## 4.2 Two-dimensional array circuit

The two-dimensional array was constructed with 100× 100 pixel circuits. Fig. 14 shows a schematic top view of the circuit. Each photoreceptor cell is capacitively coupled to four-horizontal cells in the subjacent horizontal layer. Each of the horizontal cells is resistively coupled to its four adjacent cells in the horizontal layer. Similarly, each of the bipolar cells is capacitively coupled to corrresponding cells in the neighboring four-pixels.

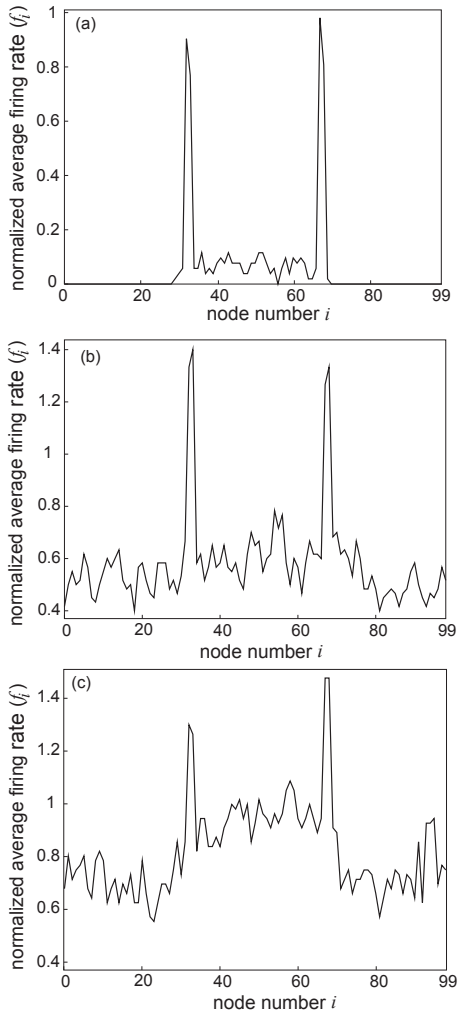


Fig. 12 Edge detection at sample temperatures: (a) Temperature T = 0 K, (b) Temperature T = 10 K, and (c) Temperature T = 20 K

### 4.2.1 Edge response

To confirm the operation of the two-dimensional circuit, a 34 × 34 pixel sized window was projected into the middle of the array circuit. The response is shown in Fig. 15. The photoreceptors receive light inputs to produce a high firing

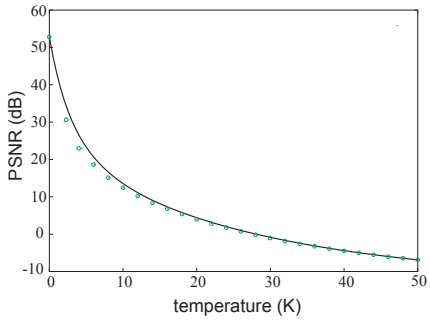


Fig. 13 Edge detection capacity (peak signal to noise ratio) for T = 0 - 50 K

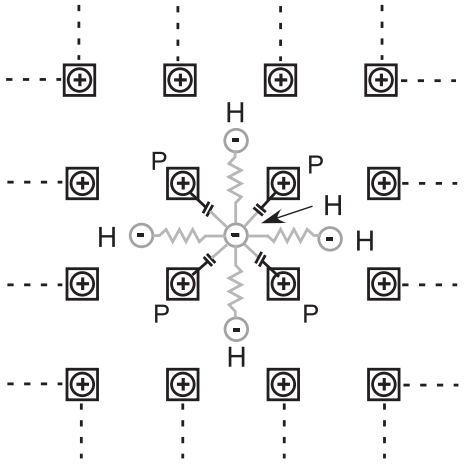


Fig. 14 Schematic of the two-dimensional circuit configuration, showing positions of photoreceptor and horizontal cells

rate (Fig. 15(a)). The horizontal cell layer response is shown in (b), while the bipolar cell output is shown in (c). We could successfully detect edges in the projected image.

### 4.2.2 Temperature characteristics

To analyse temperature characteristics of this circuit, we consider the cross section along A-B, in the middle of the input image (Fig. 16). Point "A" was taken as node number 0, while B as node number 99. The ability of the circuit to detect edges was analyzed by computing the average tunneling rates of bipolar cells along this cross section. The results are shown in Fig. 17, for T = 0 K, 5 K, and 10 K for (a), (b) and (c) respectively. The vertical axis is normalized by the maximum average firing rate of bipolar cell circuits at T = 0 K. The firing rates for all bipolar cells increase with temperature. The performance of the circuit in detecting edges in projected images over a temperature range of 0 - 20 K is shown in Fig. 18. The vertical axis represents the peak signal-to-noise ratio (PSNR) defined as:


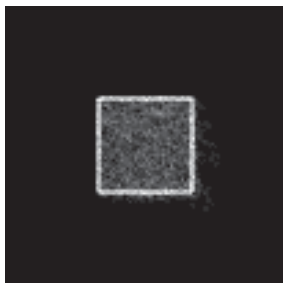


Fig. 15 Response of (a) Photoreceptors, (b) Horizontal cells, and (c) Bipolar cells to incident image (T = 0 K)

$$\text{PSNR} = 20\log_{10}\left(\frac{f_{\max}}{\sqrt{\text{MSE}}}\right) \quad (2)$$

$$\text{MSE} = \frac{1}{N^2}\sum_{i=0}^{N-1}\sum_{j=0}^{N-1}\left(f_0(i,j) - f_T(i,j)\right)^2$$

where, $f_{max}$ is the average firing rate for the entire bipolar circuit at room temperature, MSE is the mean square error, $f_0(i,j)$ is the firing rate for the $[i,j]$th node of the bipolar circuit at zero temperature (i.e. the ideal output), and $f_T(i,j)$ is the firing rate for the $[i,j]$th node of the bipolar circuit at temperature T K, and $N = 100$. The MSE was obtained by averaging five runs at each temperature. The firing rate $f_{max}$ was 11.36, normalized by the maximum firing rate for the bipolar cell layer at 0 K.

### 4.2.3 Edge enhancement in a gray image

Fig. 19 shows the edge computation results of a 100× 100 sized gray image projected onto the two-dimensional circuit.

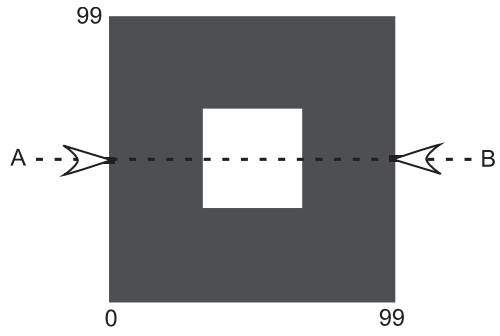


Fig. 16 Schematic diagram showing cross section "A-B" along which temperature characteristics were analyzed.

Fig. 19(a) is the input image. The dark region represents non-illuminated pixels of the array. The coloring in (b), and (c) corresponds with firing rates of the oscillators, with the dark coloring representing a zero firing rate, and the white representing a high firing rate. The edge detection results at T = 0 K, and T = 5 K are shown in Figs. 19(b) and (c) respectively. As the temperature increases, the firing rate of the entire the circuit increases. This is indicated by the grayish background in Fig. 19(c). This would increase with temperature, leading to a low edge extraction capacity.

## 5. Discussions

### 5.1 Device fabrication

Toward fabricating the proposed device, we need to address two issues. The first is controlling the position of single units (nano-dots) and fabricating the local capacitive couplings between neighboring nano-dots in the array. The second is how to fabricate large resistances on top of minute nano-dots to form single-electron oscillators. The first problem of controlling the positions of individual nano-dots could be solved as explained by one of the authors in [31], through self-organized crystal growth based on selective-area metalorganic vapor-phase epitaxy (details on the fabrication process are given in [32] and [33]). To construct single-electron oscillators, we would require a large resistance. Instead of conventional resistors, a series of tunneling junctions, i.e., multi-tunneling junction structures, could be used instead[22], and can be fabricated with the same method.

### 5.2 Improving temperature performance

Stochastic resonance is a phenomenon where weak signals can be retrieved from a noisy output [35],[34] by applying an optimal ammount of random noise. Single-electron de-

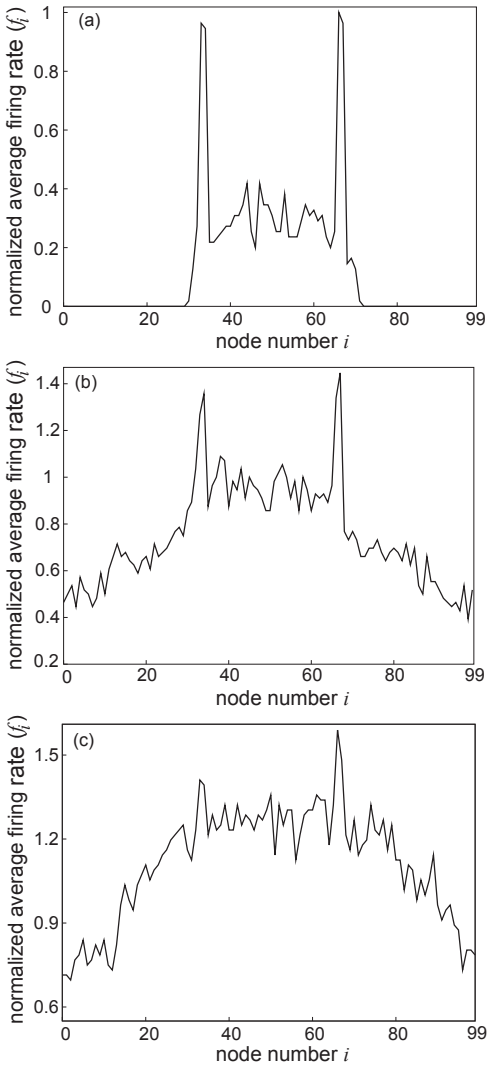


Fig. 17 Firing rates for bipolar cell circuits along cross section A-B at smple temperatures. (a) T = 0 K, (b) T = 5 K, and (c) T = 15 K

vices are sensitive to thermal noises. As shown in our results, the probability of random electron tunneling (firing) rises as the temperature increases, degrading the capacity of edge detection. One method of improving the circuit performance in relation to temperature is to utilize these thermally induced noises (random tunneling events). Living organisms are immune against noise in information processing; they effectively process information even in noisy environments [29],[30]. It is presumed that one of the ways they are able to do so is by exploiting stochastic resonance (SR) [36]. Oya et al., [37] proposed a single-electron neural network and demonstrated its improved temperature performance by em-

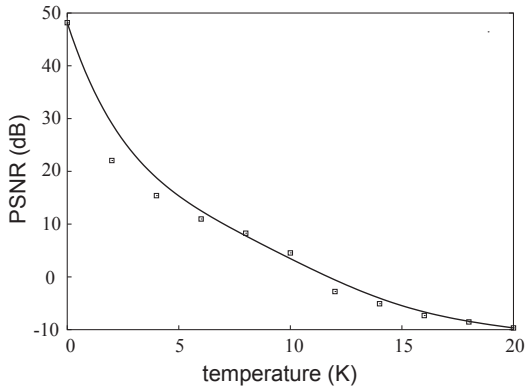


Fig. 18 Edge detection capacity (PSNR) over a temperature range of T = 0 - 20 K


Fig. 19 Edge detection results for gray image: (a) Input image, (b) and (c): Edge detection results at T = 0 K (b), and T = 5 K (c)

ploying SR in detecting output signals. This was achieved by setting the input signal to a value lower than the tunneling (firing) threshold of the neurons. By applying thermal noises, neurons with non-zero inputs were thermally induced to tunnel—tunneling events were synchronized with the input signal to a certain quantity of thermal noises. They found that the neuron performance against noises was enhanced through partially using thermal noises. We could use the same method in our edge-detecting circuit, where a number of circuit blocks would be fed with the same input. After each of the blocks processes the input image, their outputs would be summed to produce the overall output. Through this process, we could be able to successfully carry out edge detection with improved performance at higher temperatures. Therefore, applying the SR phenomenon to the proposed circuit would enhance temperature performance, hence increased PSNR against thermally induced noise, without an immediate need to find a solution through fabrication techniques.

## 6. Conclusion

Toward creating *neuromorphic architectures* with nano-electronic devices, we proposed a single-electron circuit that can detect edges in incident images. Based on a well studied retinal model, we implemented the model with single-electron devices, and confirmed its basic performance through Monte-Carlo based simulations.

## References

[1] C. Mead: Analog VLSI and Neural Systems, New York: Addison Wesley, 1989.

[2] A. Moini: Vision Chips, Kluwer, 1999.

[3] S.-C. Liu, J. Kramer, G. Indiveri, T. Delbruck and R. Douglas: Analog VLSI: Circuits and Principles, MIT Press, 2002.

[4] C. Washubber: Computational Single-Electronics, Springer, 2001.

[5] See, for example, K.K. Likharev: Single-electron devices and their applications, Proc. of IEEE, Vol. 87, pp. 606-632, 1999; and references therein.

[6] J.N. Shint, K.R. Lee and S.B. Park: Novel neural circuits based on stochastic pulse coding and noise feedback pulse coding, Int. J. of Electronics, Vol. 74, pp. 359–368, 1993.

[7] W.R. Softky and C. Koch: The highly irregular firing of cortical cells is inconsistent with temporal integration of random EPSPs, J. of Neuroscience, Vol. 14, pp. 334–350, 1993.

[8] M.N. Shadlen and W.T. Newsome: The variable discharge of cortical neurons: Implications for connectivity, computation, and information coding, J. of Neuroscience, Vol. 18, pp. 3870–3896, 1998.

[9] L. J. Croner, K. Purpura and E. Kaplan: Response variability in retinal ganglion cells of primates, Proc. Natl. Acad. Sci. USA, Vol. 90, pp. 8128-8130, 1993.

[10] N. Barkai and S. Leibler: Robustness in simple biochemical networks, Nature, Vol. 387, pp. 855–857, 1997.

[11] M. Morohashi, A.E. Winn, M.T. Borisuk, H. Bolouri, J. Doyle and H. Kitano: Robustness as a measure of plausibility in models of biochemical network, J. Theoret. Biol., Vol. 216, pp. 19-30, 2002.

[12] M.C.W. van Rossum, B. J. O'Brien and R. G. Smith: Effects of noise on the spike timing precision of retinal ganglion cells, J. Neurophysiology, Vol. 89, pp. 2406-2419, 2003.

[13] C.L. Passaglia and J.B. Troy: Impact of noise on retinal coding of visual signals, J. Neurophysiology, Vol. 92, pp. 1023-1033, 2004.

[14] J. B. Demb, P. Sterling and M. A. Freed: How retinal ganglion cells prevent synaptic noise from reaching the spike output, J. Neurophysiology, Vol. 92, pp. 2510 - 2519, 2004.

[15] H. Kitano: Biological robustness, Nat. Rev. Genet., Vol. 5, pp. 826–837, 2004.

[16] R. Douglas, M. Mahowald and C. Mead: Neuromorphic analogue VLSI, Annual Review of Neuroscience, Vol. 18, pp. 255-281, 1995.

[17] K.K. Likharev and A.B. Zorin: Theory of the Bloch-wave oscillations in small Josephson junctions, J. of Low Temp. Phys., Vol. 59, pp. 347-382, 1985.

[18] D.V. Averin and K.K. Likharev: Coulomb blockade of single-electron tunneling and coherent oscillations in small tunnel junctions, J. of Low Temp. Phys., Vol. 62, pp. 345-373, 1986.

[19] H. Gravert and M.H. Devoret: Single Charge Tunneling—Coulomb Blockade Phenomena in Nanostructures, Plenum Press, 1992.

[20] A. Fujiwara, Y. Takahashi and K. Murase: Observation of single electron-hole recombination and photon-pumped current in an asymmetric Si single-electron transistor, Phys. Rev. Lett., Vol. 78, No. 8, pp. 1532-1535, 1997.

[21] R. Nuryadi, Y. Ishikawa and M. Tabe: Single-photon-induced random telegraph signal in a two-dimensional multiple-tunnel-junction array, Phys. Rev. B, Vol. 73, pp. 45310-45316, 2006.

[22] T. Oya, T. Asai, T. Fukui and Y. Amemiya: Reaction-diffusion systems consisting of single-electron oscillators, Int. J. Unconventional Computing, Vol. 1, No. 2, pp. 177-194, 2005.

[23] T. Oya, A. Schmid, T. Asai, Y. Leblebici and Y. Amemiya: On the fault tolerance of a clustered single-electron neural network for differential enhancement, IEICE Electronics Express, Vol. 2, No. 3, pp. 76-80, 2005.

[24] T. Oya, T. Asai, R. Kagaya, T. Hirose and Y. Amemiya: Neuronal synchrony detection on signle-electron neural network, Chaos, Solitons & Fractals, Vol. 27, No. 4, pp. 887-894, 2006.

[25] E. M. LowRY and J.J. DE PALMA: Sine-wave response of the visual system. I. The Mach phenomenon, J. Opt. Soc. Am., Vol. 51, pp. 740-746, 1961.

[26] S. M. Wu, F. Gao and B. R. Maple: Functional architecture of synapses in the inner retina: segregation of visual signals by stratification of bipolar cell axon terminals, J. Neuroscience, Vol. 20, pp: 4462–4470, 2000.

[27] R. H. Masland: The fundamental plan of the retina, Nature Neuroscience, Vol. 4, pp. 877–886, 2001.

[28] R. H. Masland: Neuronal diversity in the retina, Current Opinion in Neurobiology, Vol. 11, pp. 431-436, 2001.

[29] W. R. Adey: Organization of brain tissue: Is the brain a noisy process?, Int. J. Neurosci., Vol. 3, pp. 271-284, 1972.

[30] J. J. Collins, C. C. Chow and T. T. Imhoff: Stochastic resonance without tuning, Nature, Vol. 376, pp. 236-238, 2002.

[31] T. Oya, T. Asai, T. Fukui and Y. Amemiya: A majority-logic nanodevice using a balanced pair of single-electron boxes, J. of Nanoscience and Nanotechnology, Vol. 2, No. 3/4, pp. 333-342, 2002.

[32] K. Kumakura, J. Motohisa and T. Fukui: Formation and characterization of coupled quantum dots (CQDs) by selective area metalorganic vapor phase epitaxy, J. Crystal Growth, Vol. 170, No. 1, pp. 700-704, 1997.

[33] L. Yang, J. Motohisa, J. Takeda and T. Fukui: Photonic crystal slabs with hexagonal airholes fabricated by selective area metal organic vapor phase epitaxy, Sensors and Actuators; A, Vol. 133, pp. 288-293, 2007.

[34] E. Simonotto, M. Riani, C. Seife, M. Roberts, J. Twitty and F. Moss: Visual perception of stochastic resonance, Phy. Rev. Lett., Vol. 78, No. 6, pp. 1186-1189, 1997.

[35] L. Gammaitoni, P. Hanggi, P. Jung and F. Marchesoni: Stochastic resonance, Reviews of Modern Physics, Vol. 70, No. 1, 1998.

[36] J. K. Douglass, L. Wilkens, E. Pantazelou and F. Moss: Noise enhancement of information transfer in crayfish mechanoreceptors by stochastic resonance, Nature, Vol. 365, pp. 337-340, 1993.

[37] T. Oya, T. Asai, R. Kagaya, S. Kasai and Y. Amemiya: Stochastic resonance among single-electron neurons on Schottky wrap-gate device, Int. Cong. Series, Vol. 1291, pp. 213-216, 2006.

**Andrew K. Kikombo** received the B.E. degree in electronics engineering from the University of Electro-Communications Tokyo, Japan, in 2005 and the M.S. in electrical engineering from Hokkaido University, Japan, in 2007. He is currently working toward the Ph.D. degree in electrical engineering at Hokkaido University, Japan. His research interests include modeling, design and simulation of bio-inspired single-electron circuits. Mr. Kikombo is a member of the Japan Society of Applied Physics.

**Alexandre Schmid** received the M.S. degree in microengineering and the Ph.D. degree in electrical engineering from the Swiss Federal Institute of Technology (EPFL) in 1994 and 2000, respectively. He has been with the EPFL since 1994, working at the Integrated Systems Laboratory as a research and teaching assistant, and at the Electronics Laboratories as a post-doctoral fellow. His earlier work included the development and modeling of digital and mixed analog-digital circuits for video processing, delta-sigma converters and neuromorphic applications. He joined the Microelectronic Systems Laboratory in 2002 as a Senior Research Associate, where he has been conducting research in the fields of non-conventional signal processing hardware, reliability of nanoelectronic devices, and bioelectronic interfaces. Dr. Schmid is also teaching at the Microengineering and Electrical Engineering Departments of EPFL.

**Tetsuya Asai** is an Associate Professor in the Graduate School of Information Science and Technology, Hokkaido University, Sapporo, Japan. His research interests concentrate around developing nature-inspired integrated circuits and their computational applications. Current topics that he is involved with include; intelligent image sensors that incorporate biological visual systems or cellular automata in the chip, neuro chips that implement neural elements (neurons, synapses, etc.) and neuromorphic networks, and reaction-diffusion chips that imitate vital chemical systems.

**Yusuf Leblebici** received the B.S. and M.S. degrees in electrical engineering from Istanbul Technical University, Istanbul, Turkey, in 1984 and 1986, respectively, and the Ph.D. degree in electrical and computer engineering from the University of Illinois at Urbana-Champaign in 1990. Between 1991 and 2001, he worked as a faculty member at UIUC, at Istanbul Technical University, and at Worcester Polytechnic Institute (WPI), where he established and directed the VLSI Design Laboratory, and also served as a project director at the New England Center for Analog and Mixed-Signal IC Design. Since 2002, he has been a Chair Professor at the Swiss Federal Institute of Technology in Lausanne (EPFL), Switzerland, and Director of Microelectronic Systems Laboratory. His research interests include design of high-speed CMOS digital and mixed-signal integrated circuits, computer-aided design of VLSI systems, intelligent sensor interfaces, modeling and simulation of semiconductor devices, and VLSI reliability issues.

**Yoshihito Amemiya** received the B.E., M.E., and Ph.D. degrees from the Tokyo Institute of Technology, Tokyo, Japan, in 1970, 1972, and 1975. He joined NTT Musashino Laboratories in 1975, where he worked on the development of silicon process technologies for high-speed logic LSIs. From 1983 to 1993, he was with NTT Atsugi Laboratories and developed bipolar and CMOS circuits for Boolean logic LSIs, neural network LSIs, and cellular automaton LSIs. Since 1993, he has been a Professor with the Department of Electrical Engineering, Hokkaido University, Sapporo. His research interests are in the fields of silicon LSI circuits, signal processing devices based on nonlinear analog computation, logic systems consisting of single-electron circuits, and information-processing devices making use of quantum nanostructures.

(Received May 12, 2008; revised August 26, 2008)